Journal Name

ARTICLE TYPE

Cite this: DOI: 10.1039/xxxxxxxxxx

Water Structure and Dynamics in the Hydration Layer of a Type III Anti-freeze Protein†

Z. Faidon Brotzakis,[a‡] Ilja K. Voets, [b], Huib J. Bakker [c], and Peter G. Bolhuis [*a]

Received Date
Accepted Date

DOI: 10.1039/xxxxxxxxxx

www.rsc.org/journalname

We report on a molecular dynamics study on the relation between the structure and the orientational (and hydrogen bond) dynamics of hydration water around the ocean pout AFP III anti-freeze protein. We find evidence for an increasing tetrahedral structure from the area opposite to the ice binding site (IBS) towards the protein IBS, with the strongest signal of tetrahedral structure around the THR-18 residue of the IBS. The tetrahedral structural parameter mostly positively correlate with increased reorientation decay times. Interestingly, for several key (polar) residues that are not part of the IBS but are in its vicinity, we observe a decrease of the reorientation time with increasing tetrahedral structure. A similar anti-correlation is observed for hydrogen-bonded water molecules. These effects are enhanced at lower temperature. We interpret these results in terms of structure-making and structure-breaking residues. Moreover, we investigate the tetrahedral structure and dynamics of waters at a partially dehydrated IBS, and for the protein adsorbed at the air-water interface. We find that the mutation changes the preferred protein orientation upon adsorption at an air-water interface. These results are in agreement with water-air Vibration Sum Frequency Generation spectroscopic experiments showing a strongly reduced tetrahedral signal upon mutation at the IBS.

1 Introduction

The structure and dynamics of a protein's hydration layer is crucial for its functioning and conformational dynamics. Hydration plays an active role in biological processes such as protein folding, ligand binding, and protein recognition[1–3]. Protein-solvent interactions are especially important in antifreeze proteins (AFP), as they have to specifically recognize and bind — through their Ice Binding Site (IBS) — nucleating ice crystals in the excess of liquid water and prevent further growth of ice[4]. In spite of this seemingly tough goal AFPs show a large structural diversity in nature and are seen in many organisms such as fungi, bacteria, fish, insects, where their major function is to help these organisms survive at subzero temperatures[5]. In addition to their biological role, AFPs also have a variety of applications as ice avoiding agents, from organ preservation[6] to texture enhancers in food[7].

Many AFPs are characterized by an IBS consisting of regular beta-sheets or spirals, commensurate with the ice-crystal planes. A counterexample is the ocean pout AFP III that does not exhibit a regular beta sheet ice binding site, raising the question of how the binding to ice is achieved instead.

Both simulations[8–10] and experiments[11–13] indicate that water is more structured at the IBS with respect to other non-IBS sites of the ocean pout AFP III protein (hereafter shortened to AFP III). The type of interactions necessary for the affinity and specificity of the IBS to ice crystals have been addressed by mutation studies, X-ray crystallography[13,14] and simulations[8,9,15]. There is an increasing consensus on the combined role of both polar groups (able to form hydrogen bonds) and apolar groups in ice binding by matching to ice-lattice oxygens as well as by hydrophobic ice-IBS interactions. Moreover, for a β-helical anti-freeze protein, Nutt el al[16] pointed out that not only the IBS is important for ice recognition but also the non-IBS residues, which distort the tetrahedral water structure.

AFP III's ice-binding-site is relatively flat and hydrophobic, thus serving as a great candidate for surface sensitive interface experiments. In particular, Vibration Sum Frequency Generation (VSFG) spectroscopy can be used to study water structure at interfaces by measuring its OH stretch vibration. A recent study[17] of the ocean pout AFP III protein adsorbed at a water-air interface observed a predominant OH stretch vibration signal at 3200

[a] Van 't Hoff Institute for Molecular Sciences, Universiteit van Amsterdam, Science Park 904, 1098 XH Amsterdam, The Netherlands; E-mail: p.g.bolhuis@uva.nl
[b] Laboratory of Macromolecular and Organic Chemistry, Laboratory of Physical Chemistry, and Institute for Complex Molecular Systems, Eindhoven University of Technology, PO Box 513, 5600 MB, Eindhoven, Netherlands.
[c] FOM Institute AMOLF, Science Park 104, 1098 XG Amsterdam, The Netherlands
† Electronic Supplementary Information (ESI) available: See DOI: 10.1039/b000000x/
‡Present address: Department of Chemistry and Applied Bioscience, ETH Zürich and Facoltà di Informatica, Istituto di Scienze Computazionali, Universita della Svizzera Italiana, Via Buffi 13 Lugano, CH-6900, Lugano, Switzerland.

cm^{-1}, indicating enhanced ice-like order. A single point mutation of a core IBS amino acid from THR-18 into ASN-18, resulted in a loss of this ice-like signal, as well as of the anti-freeze activity of the AFP III. The effect of this mutation on the water structure and dynamics is not known in full detail.

Here, we employ all atom molecular dynamics (MD) simulations to obtain microscopic insight in the tetrahedral structure and reorientation dynamics of the protein hydration layer for the wild type and the T18N mutant. The aim of this work is twofold. First we establish a relation between the water reorientation dynamics and tetrahedral water structure at different parts of the protein hydration layer, and interpret this in terms of tetrahedral structure-making and -breaking ability of the individual residues. We find that the mutant alters the hydration layer structural and dynamical properties, but only slightly, and seemingly not sufficient to explain the strong signal decrease in the VSFG experiment. Therefore, a second aim of this work is to investigate a possible alternative explanation, namely that the mutation changes the adsorption properties of the protein to the water-air interface. As the VSFG experiments were surface sensitive, most of the signal is caused by water at the hydrophobic surface of the protein exposed to the water-air interface. We mimic this exposure of the protein to air by studying a partially dehydrated IBS as well as explicitly simulating an air-water interface. We find evidence that structured water at the IBS surface of the wild type is exposed to the air-water interface, leading to a strong VSFG signal, while the mutant IBS surface is turned away from the air-water surface, therefore contributing less to the signal. Hence, we offer an alternative interpretation of the VSFG results.

The paper is structured as follows. We start with a methodology section in which we give the simulation details, and (re)introduce the framework to study water reorientation dynamics. This is followed by a description of the water structural parameters. Next, we present the results on water reorientation dynamics and tetrahedral structure at different sites of the surface of a wild type and mutant type AFP III, followed by a discussion on the correlation between these two observables. Finally, we compare water reorientation dynamics and tetrahedral structure for a dehydrated wild type and mutant AFP III, as well as their absorption propensity to a water-air interface, which we discuss in the light of VSFG experiments. We end with concluding remarks.

2 Methodology

2.1 Simulation details

We employed Gromacs 4.5.4[18] for performing molecular dynamics simulations. The ocean pout wild type (WT) monomer structure was obtained from PDB 1HG7[19] and the mutated ocean pout structure (THR-18 to ASN-18) was obtained from PDB 1JAB[20]. We solvated each structure with SPC/E or TIP4P/2005 water models. The choice of two different water models serves, not so much as a comparative study of the two models, but as a consistency test. SPC/E water model is known to better reproduce the dielectric constant of water[21] than TIP4P/2005, but that the latter model better reproduces phase behavior. In previous work we found that the SPC/E model describes the water orientation dynamics reasonably well[22]. Therefore, in the main text, we report the results for the SPC/E water model unless stated otherwise. The results of the TIP4P/2005 model are given in in the ESI†.

The protein all atom interactions were described using the amber99sb-ildn force field[23]. Hydrogen atoms were added, and residue protonation states were set according to their value at neutral pH. Hence, the protonation state of the amino acids corresponds to a pH of 7. Upon solvating the resulting cubic simulation box with a side length of 5.9 nm contained 7228 solvent molecules. No ions needed to be added to the solution after assigning hydrogens to the pdb structures since the total charge of both structures was zero. After energy minimization, both water force-field systems were equilibrated for 1 ns at a constant pressure of 1 atm and at several temperatures. These temperature were 298 K, 285 K, 270 K, 255 K, 240 K, 225 K and 1 atm for the SPC/E systems and 298 K, 285 K, 270 K, 255 K for the TIP4P/2005 systems. For each temperature and water model we launched one MD production simulation of 100 ns in the NPT ensemble.

The MD simulation settings were the same as in a previous study[22]. We used Lincs for constraining the bonds. We employed a 1 nm cutoff for the Lennard-Jones interactions, and treated the electrostatics by using the Particle Mesh Ewald with a short range cutoff of 1 nm and a Fourier spacing of 0.12 nm. Updating of neighbor lists (cutoff 1 nm) occurred every 10 fs. We used the leap-frog integration scheme with a standard time-step of 2 fs[23]. Moreover, the v-rescale thermostat[24] was used for temperature coupling and the Parrinello-Rahman barostat[25] for pressure coupling, with time constants 0.2 ps and 1.0 ps, respectively.

To ensure that the dynamics is unaffected by the thermostat and/or barostat, we perform and analyze NVE trajectories. For each temperature, from the 100 ns long MD trajectory in the NPT ensemble, we selected 10 frames with instantaneous energy and volume equal to their respective averages, and performed individual 1 ns NVE simulations. Switching functions were applied to the non-bonded interactions from 0.8 nm with a cutoff of 1.0 nm. In these runs, we prevented energy drift by setting the time step to 1 fs. The energy was calculated every 10 fs and the frame saving frequency was 100 fs.

In this paper the solvated wild type and mutant will be denoted as fully hydrated systems. The effect of water dehydration on the water structure and dynamics was investigated by analyzing partially dehydrated systems. For each combination of temperature, water force field, and WT/mutant, we took the last frame of the 100 ns NPT MD trajectory and reduced the water content by about a factor of 10, leaving only 722 protein surface water molecules. We ran another 100 ns NVT at the same temperatures as the fully hydrated systems. From each of these NVT trajectories, we selected 10 frames with instantaneous energy and temperature equal to the average ones and performed individual 1 ns NVE simulations. The other parameters for the NVT and NVE of the dehydrated systems were identical to those of the fully hydrated systems.

In order to investigate the affinity of WT/T18N proteins to an air/water interface in a slab geometry, we also built two solvated systems of WT and T18N with identical cubic box sizes, and simi-

lar number of water molecules (around 6500). After energy minimization and water (SPC/E) equilibration, for each system we extended the simulation box in the z-direction by a factor three, thus creating two water-vapor interfaces. Using this as an initial configuration, we started three independent NVT simulations at room temperature for each system. The used parameters were identical to the ones mentioned above, except for a "force and potential correction applied in the z-dimension to produce a pseudo-2D summation"[18].

2.2 Hydrogen bond lifetimes

Throughout this paper we abbreviate hydrogen bonds as H-bonds. As in our previous study[22], we took the standard H-bond definition parameters (donor-acceptor distance ≤ 0.35 nm and acceptor-donor-hydrogen angle $\leq 30°$) as these parameters fall close to the water water hydrogen bond saddle point value[26,27]. We allowed for two types of hydrogen bond breakage mechanisms, a hydrogen bond exchange mechanism[28] and a translational diffusion mechanism[22,29]. In the first mechanism the H-bond lifetime is defined as the time required for water OH to fully exchange its hydrogen bond acceptor, while in the second mechanism it is the time needed for the H-bond to break but remain dangling for at least 200 fs.

2.3 Water reorientation dynamics

The reorientation dynamics of an ensemble of water molecules can be represented using the time correlation function[22,30,31]

$$C_2(t) = \frac{2}{5}\langle P_2[\mathbf{u}(0)\cdot\mathbf{u}(t)]\rangle, \qquad (1)$$

by tracing the dynamics of water OH bond vector $\mathbf{u}$ through the second Legendre polynomial time correlation function. This can be related to anisotropy decay curves from time-resolved infrared spectroscopy and to orientation relaxation times obtained from NMR[31].

Since we are interested in the reorientation dynamics of water at the vicinity of various protein-surface sites, we also calculated the anisotropy decay curve

$$c_j^m(t) = \frac{1}{5\ell}\sum_{t'=t_0^m}^{t_0^m+\ell\Delta t}\sum_{k=1}^{2} P_2[\mathbf{u}_{jk}(t')\cdot\mathbf{u}_{jk}(t'+t)] \qquad (2)$$

of both OHs ($k = 1,2$) of an individual water molecule j for intervals of duration $\ell\Delta t$ that the water's oxygen atom is within 4.4 Å distance of the heavy atoms of the protein, where t_0^m is the start of the mth interval. In this analysis we allowed the oxygens to undergo nonessential excursions outside the hydration layer for less than 2 ps. Thereafter a single exponential fit is performed to Eq. 2 in the interval 0-10 ps and yielding a separate time τ_j^m for each water molecule residing for time $\ell\Delta t$ in the vicinity of the protein. One can attribute that reorientation time to a particular amino-acid #AA with a weight $\ell f_{\#AA}$, where $f_{\#AA}$ is the frame fraction in the interval ℓ where water j was within 4.4 Å of a particular amino-acid #AA.

2.4 Water structure and dynamics at different areas of the protein

Based on mutation studies by Graether et al[20] we define six different parts of the protein surface, the residues THR-18 and ASN-18, the IBS, the vicinity and the opposite face, the non-IBS residues (everything but the IBS), and the entire hydration shell which consists of the IBS and non-IBS (see Fig. 1 for an illustration). The vicinity and opposite face residues were selected to include key surface residues identified in Ref.[20]. They include vicinity residues 39,42,46,47,61 and opposite residue 29. Figure 1 shows which residues of the protein surface belong to the IBS, the vicinity and the opposite group. Rendered in blue are the IBS residues 9,10,12, 13, 14, 15, 16, 18, 19, 20, 21, 44. Depicted in magenta are the vicinity residues within 0.4 nm of the IBS 8, 23, 37, 39, 42, 43, 46, 47, 48, 50, 51, 61). The green opposite site residues are 1.5 nm away of the IBS and include residues 0, 1, 2, 26, 27, 28, 29, 30, 56.

2.5 Tetrahedral structural parameter S

Sharp and coworkers[9,32,33] introduced a method to identify the tetrahedral structuring of water around amino acids based on the distribution of a water-water angle. In a given frame one calculates for each amino acid the minimum water-water OOH angle θ (see Fig. 2 for a graphical definition) for all water-water pairs within 3.5 Å from each other and solvating that amino acid. The distribution $P(\theta)$ of these angles shows a bimodal distribution with a minimum at 30° (see Fig. 5a), distinguishing between tetrahedral water population (angles lower than 30°) and a perturbed H-bond network, mostly occurring around hydrophilic groups ($\theta > 30°$). The tetrahedral structure parameter S is then defined as the integral of $P(\theta)$ up to $\theta = 30°$.

It turns out that water around hydrophobic groups have a larger S due to smaller H-bond angles θ, inducing stronger water-water bonds, with bigger energy fluctuations and therefore a positive heat capacity of the solvating water. Conversely, the introduction of a hydrophilic group around water strains the water-water H-bond angle and shifts the angle distribution to higher values, and hence a lower S, thus decreasing the water-water bond energy and fluctuations which decreases the heat capacity of solva-

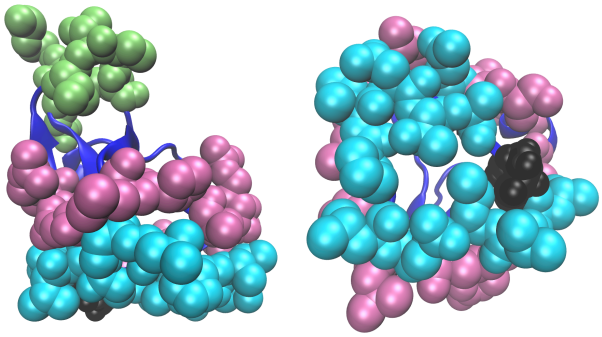

Fig. 1 Partitioning of the protein into three distinct areas. The area IBS (denoted by cyan), vicinity (denoted by magenta) and opposite (denoted by green). THR-18 is denoted by black.

tion[9,32,33].

Throughout the text we will associate tetrahedrally structured water with a large S value (high tetrahedral water population) and unstructured water with a low S value (low tetrahedral water population). Unstructured water coinciding with slow reorientation dynamics will be labeled as *glass-like* water. Residues solvated by tetrahedral water will be labeled as *tetrahedral structure makers* and the ones by glass-like waters, *tetrahedral structure breakers*.

Besides the tetrahedral structural parameter S, we also used the tetrahedral order parameter q[34], and an order parameter based on the local structure index LSI [35] to identify the structure of the protein hydration layer (see ESI†). While all three can be used to see the difference between bulk water and ice-like structures, they measure different aspects of water order.

2.6 Structural parameter - water reorientation time correlation

To assess the correlation between structure and dynamics we constructed several 2D distributions. As mentioned above, each water i surrounding one amino acid for an mth interval of length ℓ, has a reorientation decay time $\tau_{i,m}$ associated with it. In this mth interval we also calculated the distribution $P(\theta_{ij})$ of the angle θ_{ij} of waters j within 3.5 Å of i and hydrating the same amino acid. From the normalized distribution $P(\theta_i) = \sum_j P(\theta_{ij}) / \sum_{i,j} P(\theta_{ij})$ we obtain the structural parameter $S_{i,m}$ for each water i hydrating a particular amino acid, by integrating from 0° to 30°. We bin the pair $\tau_{i,m}$ and $S_{i,m}$ for each residue in a 2D histogram, in order to investigate possible correlation between water tetrahedral structuring and reorientation dynamics.

The correlation of τ with the other two structural order parameters is described in the ESI†.

3 Results and Discussion

3.1 Water reorientation dynamics slows down at surface

From the MD simulations trajectories we calculated the anisotropy correlation function $C_2(t)$ using Eq. (1) for all water molecules in the system and for the hydration shell water molecules only, for both wild type and mutant at different temperatures. Fig. 3 shows these correlation functions for the SPC/E model. (See the ESI† for the TIP4P/2005 results). As expected the anisotropy for all waters decays within a few ps for ambient conditions, but slower with decreasing temperature. This agrees with the work of Stirnemann et al[36], who found that the decay

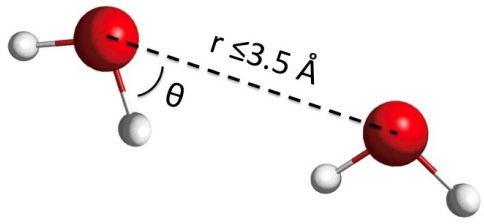

Fig. 2 Definition of the θ angle.

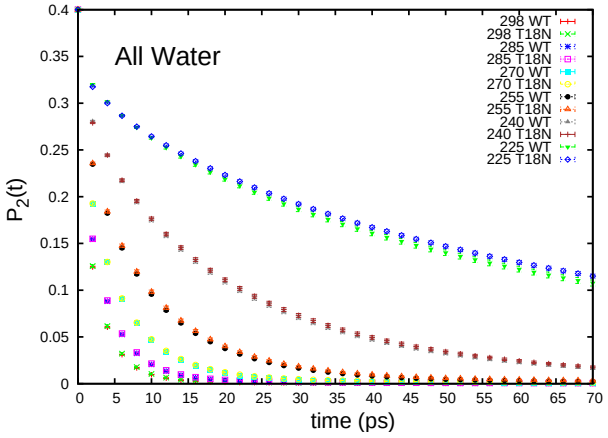

(a)

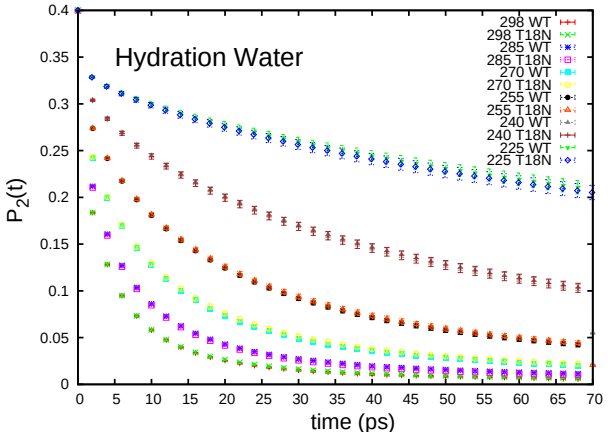

(b)

Fig. 3 Anisotropy decay of a) all water and b)the hydration shell water of the wild type and mutant SPC/E systems.

time becomes longer upon cooling. For the hydration water this effect is even more striking.

3.2 Water reorientation dynamics local differences

Although the hydration shell water reorients slower than bulk water (see Figs. 3 and 4), the difference in overall hydration water reorientation dynamics between mutant and wild type is surprisingly small (see Fig. 3). This indicates that the effect of the mutation on the water reorientation dynamics is either small and/or local, since the number of waters hydrating THR-18 and ASN-18 is small compared to the total amount of waters in the hydration shell, washing out any local effect. To study whether THR-18 and ASN-18 differ significantly in local water dynamics we therefore categorized the hydration water by their local environment (see Methodology section 2.4). In Figure 4a, we plot the water orientation decay time τ for the six different parts of the protein. Xu et al[37] discovered a small acceleration of the H-bond dynamics upon mutating ALA-16 to HIS-16. Here we find that water reorients significantly slower around THR-18 than around other regions, and also slower than at the mutated site ASN-18. This effect is enhanced at lower temperatures (see Fig. S3 of the ESI†). However, the point mutation does not drastically accelerate the reorienta-

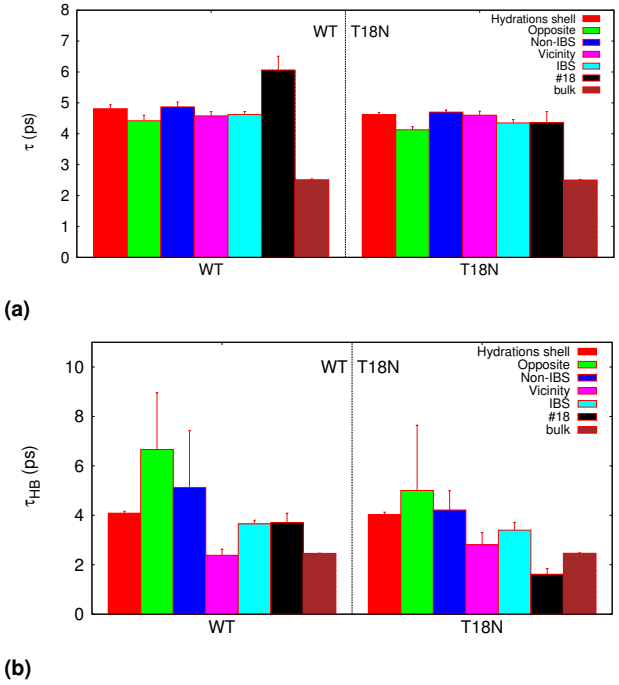

Fig. 4 a) Water reorientation time, b) protein water H-bond lifetimes of hydration water for SPC/E systems of a wild type (WT), and mutant (T18N) at room temperature. Color coding as in Fig. 1.

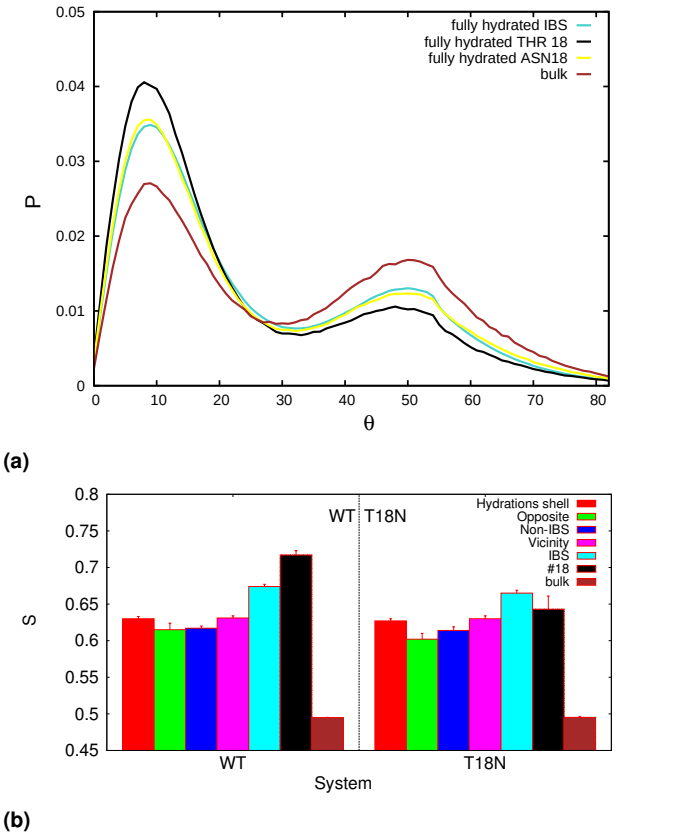

Fig. 5 a) OOH angle distribution of water pairs solvating the wild fully hydrated system IBS (cyan) , THR-18 of the wild fully hydrated system (black) , ASN-18 of the mutant fully hydrated system (yellow), of the bulk water (brown). b) Structure order parameter of water (S), for the different parts of the protein. All the above systems are in room temperature and for the SPC/E water systems. Color coding as in Fig. 1.

tion dynamics of the IBS, but only has a local effect. This local acceleration of water reorientation dynamics around ASN-18 coincides with the less stable water-ASN-18 hydrogen bonds, compared to both the water-THR-18 ones, and to bulk water-water H-bonds (see Fig. 4b). This effect is again enhanced at lower temperatures (see Fig. S4).

X-ray crystallography mutation studies by Graether et al[20] and Neutron scattering experiments by Howard et al [13], have indicated the central role of the THR-18 side chain OH in matching the ice plane and therefore in the anti-freeze activity of the molecule. Threonine's side chain OH group actively participates through a H-bond with water. These findings are in agreement with our results which show that upon substitution of the THR-18 side chain to an ASN-18, the hydrogen bond and reorientation around ASN-18, becomes faster.

3.3 Hydration water structure

Following Sharp and Gallagher[9,33] and other authors[10], we characterize the water structure by computing the minimum OOH angle distribution for several parts of the protein (see Fig. 5a), from which we obtain the average water structural parameter S. Figure 5b shows the average water structural parameter S for the overall hydration shell, the IBS, the vicinity, the opposite region, and residue 18, for the WT and T18N systems. Interestingly, there seems to be a monotonic increase of water structure along the protein, i.e. the water structural parameters obey the relation $S_{bulk} < S_{opp} < S_{vicinity} < S_{IBS}$. This effect is more pronounced in the wild type system, compared to the mutant system. Both the absolute values of S and the difference $S_{IBS} - S_{opposite}$ increases slightly upon cooling (see Fig. S5 of the ESI†). This behaviour holds for both water models.

Water is more structured around the IBS and in particular residue 18 of the wild type, compared to the mutant, especially at low temperatures (see Figure S5). Thus, for the wild type system water around residue 18 not only reorients slower but also have more tetrahedral structure compared to the mutant.

These findings seem to agree with the VSFG experiments[17], which showed a drastic decrease in ice like water signal for the mutant compared to the wild type system. However, while we observe a reduction of tetrahedral water structure around THR-18 upon mutation, the reduction in the IBS tetrahedral water structure going from the wild type to mutant is not as large as the experiments suggest.

3.4 Tetrahedral structure - reorientation time correlation

We investigate the correlation between the water reorientation dynamics and tetrahedral structure by histogramming the hydrating waters as function of their $S_{i\ell}$ (or $S_{\mathrm{lsi},i\ell}$ or $q_{i\ell}$) and $\tau_{i\ell}$ in which we multiply each entry with a weight ℓ (see Method section).

Figures 6 and 7 show the 2D histograms of $S_{i\ell}$ and $\tau_{i\ell}$ of the IBS and of selected amino acids for, respectively, 298 K and 270 K for the wild type and mutant SPC/E system. At room temper-

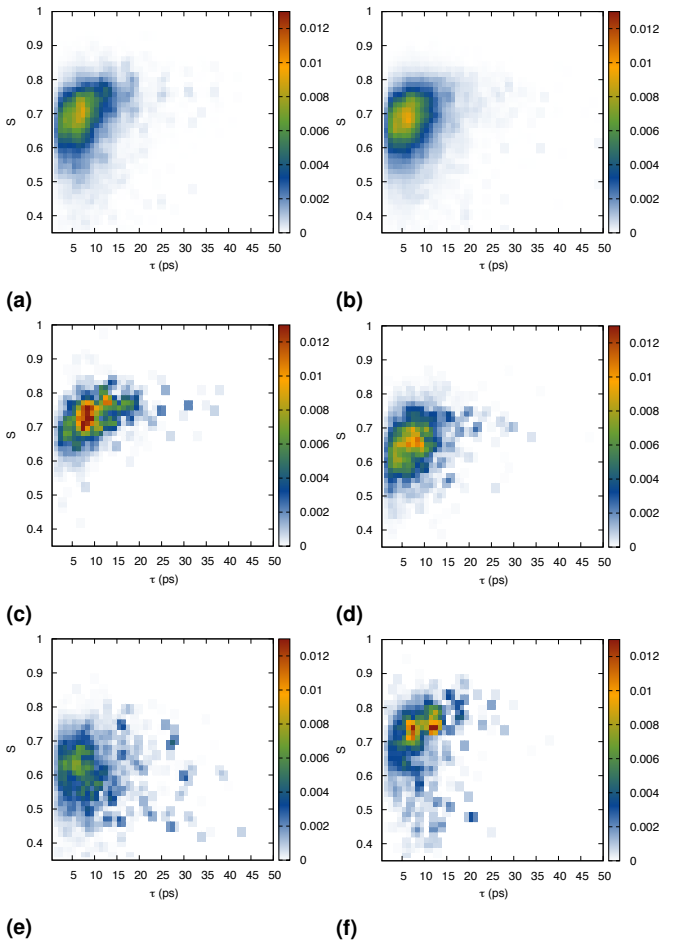

Fig. 6 Structural parameter S as a function of water reorientation decay time for selected residues of a) IBS (WT), b) IBS (T18N), c) THR-18 (WT), d) ASN-18 (T18N), e) ARG-39 (WT/vicinity), f) ALA-48 (WT/vicinity) at 298 K.

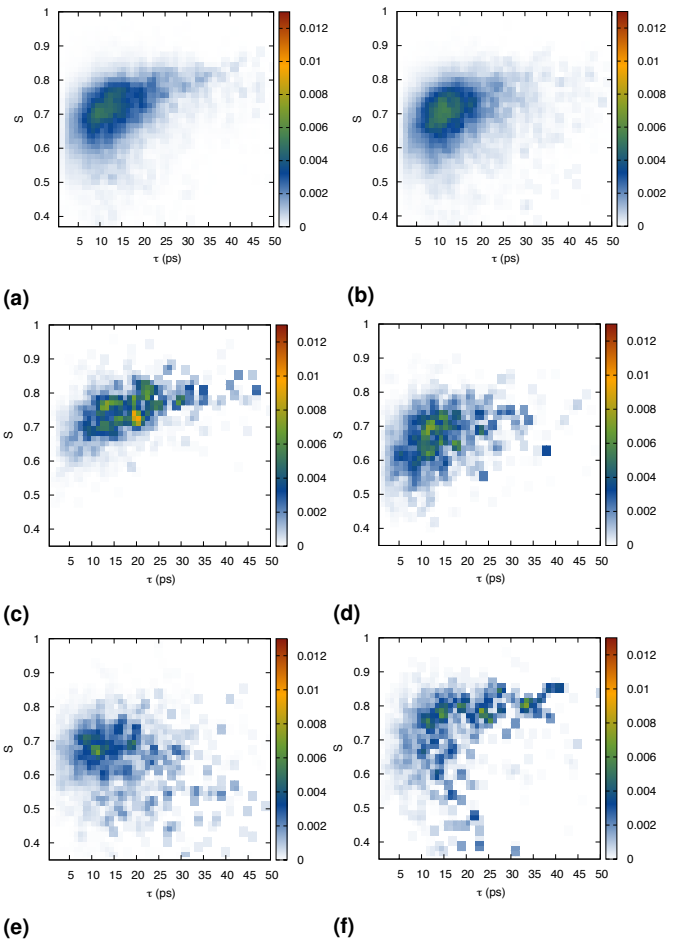

Fig. 7 Structural parameter S as a function of water reorientation decay time for selected residues of a) IBS (WT), b) IBS (T18N), c) THR-18 (WT), d) ASN-18 (T18N), e) ARG-39 (WT/vicinity), f) ALA-48 (WT/vicinity) at 270 K.

ature (Fig. 6a) the IBS of the wild type shows clearly a positive correlation between tetrahedral structure S and water reorientation time (τ). While this correlation is far from perfect, a more structured water is more likely to exhibit a longer reorientation time. Upon mutation (Fig. 6b) the IBS $S-\tau$ distribution shifts to slightly lower S and τ, and the correlation becomes less pronounced. More strikingly, water hydrating the THR-18 (WT system) shows higher values for S and τ as well as a stronger $S-\tau$ positive correlation compared to ASN-18 (T18N system). (see Figs. 6c and 6d respectively). Clearly, more tetrahedrally structured waters also reorient much slower. These positive correlations can be contrasted with the behavior of other key residues in the vicinity region of the IBS. For instance, the charged and hydrogen bond donating residue ARG-39 exhibits no or even a negative correlation between structure and dynamics (with a lower peak in S compared to THR-18). Here, less structured water shows a longer reorientation time. Interestingly, water around ALA-48 is able to exhibit both tetrahedral and glass-like structure. ALA-48 is next to ARG-47, which is a charged amino acid capable of donating hydrogen bonds.

Upon cooling the systems to 270 K, the WT (S-τ) correlation at the IBS becomes stronger compared to room temperature (Fig. 7a). Since the S-τ correlation signals at 270 K are enhanced, we can more clearly distinguish between strong tetrahedral structure making and subtle tetrahedral structure making residues at the WT-IBS. As shown in Figure S12 of the ESI† for the WT-IBS residues, there exist amino acids that show a very strong positive S-τ correlation (LEU-10, PRO-12, ILE-13, ALA-16, THR-15, THR-18, MET-21), amino acids that show a subtle S-τ correlation (GLN-9, ASN-14, LEU-19,VAL-20 and GLN-44), as well as non-IBS amino acids which show an anti-correlation (ARG-23,ASP-58). At 270 K, the point mutation results in a weaker S-τ correlation for water around the T18N-IBS (see Fig. 7b). As shown in Fig. 7c,d, S12 and S13 of the ESI†, the decreased (S-τ) correlation in the T18N IBS compared to the WT IBS can be predominantly attributed to the decreased (S-τ) positive correlation of GLN-9, LEU-10, PRO-12, THR-15, ALA-16, ASN-18, MET-21. Again, as shown in Fig. 7e, the charged and hydrogen bond donating residue ARG-39 of the vicinity region exhibits a negative correlation (with a peak at lower S compared to THR-18), and water around ALA-48 exhibits both tetrahedral and glass-like structure (Fig. 7e).

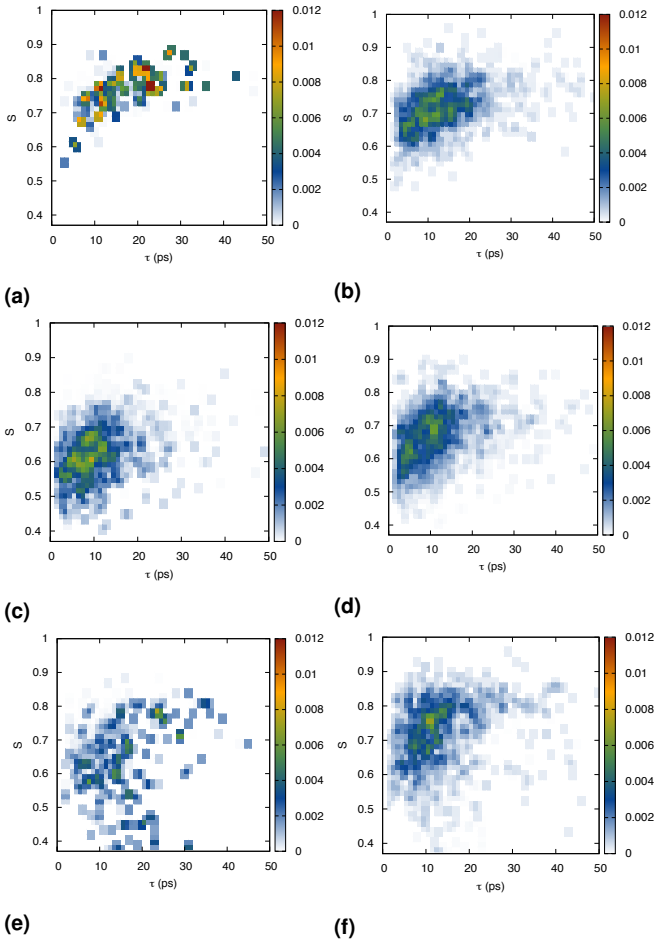

Fig. 8 Structural parameter S as a function of water reorientation decay time for residue 18 for a) THR-18 (WT) H-bonded, b) THR-18 (WT) non H-bonded, c) ASN-18 (T18N) H-bonded, d) ASN-18 (T18N) non H-bonded, e) ALA-48 (WT) H-bonded, f) ALA-48 (WT) non H-bonded,

In order to investigate which sites of ALA-48 are responsible for causing the tetrahedral and glass-like water structure, we traced the waters hydrating ALA-48 in the WT system at 270 K and identified the tetrahedral waters (S >0.75 and τ >25 ps) and glass-like water (S< 0.6 and τ >15 ps). Inspection of representative configurations (see Figure S14 of the ESI†) revealed that the tetrahedrally structured waters are hydrating the methyl group side chain of ALA-48 side chain as well as the methyl group side chains of PRO-12 and LEU-13 (Figure S14c,d), while the glass like water forms a hydrogen bond with the neighbouring charged residue ARG-47 and/or donate a hydrogen bond to the ALA-48 carbonyl (see Figure S14a,b).

This suggest that the water structure and dynamics can depend on the hydrogen bonding to the protein. To investigate this for residue THR-18 we therefore split the distribution into a hydrogen bonded population and a populating that is not hydrogen bonded to the protein. The results are plotted in figure Fig. 8. A striking result is that the h-bonded waters THR-18 show a strong positive correlation of $S-\tau$ which completely disappears for the mutant. In contrast the non-bonded population is much less affected. Moreover the situation is reversed for the vicinity residues, where the hydrogen bonded population show a lower structures than the non-bonded population .

So, we conclude that hydrated water that is hydrogen bonded to the protein at the THR-18 combines an increased tetrahedral structural order with slower reorientation, while the non-bonded waters have a lower tetrahedral structure with reorientation time. The mutation shifts this distribution towards lower tetrahedral structure with shorter reorientation times, reducing the affinity to ice crystal planes. In contrast the residues in the vicinity show the opposite behavior, with H-bonded water having a lower structure-dynamics compared to the non H-bonded waters.

Analysis using the alternative order parameters leads to similar conclusions (see ESI†). Note that both the local structure index *LSI* based parameter and the tetrahedral order parameter q, are less capable of discriminating between the different types of residue.

3.5 Structure makers versus structure breakers

The above discussion suggests that vicinity residues such as ARG-39, ALA-48, ARG-23, and ASP-58 are involved in weaker hydrogen bonds, as indicated by the shorter hydrogen bond lifetime (see Fig. 4b). At the same time, these residues exhibit a population of strongly bound hydration waters with a reduced tetrahedral structure of water, and simultaneously a slower water (reorientation) dynamics, as indicated by the negative $(S-\tau)$correlations. Such residues can thus be labeled water 'structure breakers'. It follows that there exist "tetrahedral structure making" (hydrophobic) and "tetrahedral structure breaking" residues (hydrophilic h-bond makers) which influence the structure and dynamics of water near the IBS and in the vicinity of the IBS. The tetrahedral structure making residues should have a stronger affinity for ice, while the structure breaking residues would have a lower affinity to ice crystal planes. This is in agreement with the proposed adsorption mechanism in which AFPs form anchored clathrate-like waters at their IBS; a tetrahedral layer that recognizes ice-planes[38]. The point mutation clearly introduces a structure breaking residue into the IBS, which induces a more negative $S-\tau$ correlation at the IBS, indicating a decrease in tetrahedrality and therefore a lower affinity of the IBS for ice. While slower orientation dynamics is not directly related to ice binding affinity since the latter is a equilibrium property, the reorientation dynamics is indicative of the strength of hydrogen bond. Indeed, in our previous work we showed experimentally that waters located in concave sites on the protein surface have less and weaker hydrogen bonds with slower dynamics[22]. These slower waters also have less tetrahedral structure, thus accounting for the observed negative correlation.

Our findings give additional insight by exposing a correlation between angular tetrahedral structure and water reorientation dynamics in the hydration layer around the IBS of AFP III. We speculate that water in the vicinity around the IBS should exhibit structure breaking behaviour in order for ice to bind only to the IBS and not to the surrounding parts, thus prohibiting crystal growth around the entire protein. This hypothesis matches with observations by NMR experiments that only the IBS hydra-

tion water forms ice at subzero temperatures while the rest of the protein hydration shell remains liquid [12], an effect that has been largely attributed to the disruption of tetrahedral structure caused by hydrophilic residues at an insect protein [16], or glycoproteins [39].

3.6 Effect of dehydration

The VSFG experiments that inspired this investigation probe the air water surface, where the symmetry of the system is broken [17]. It is reasonable to assume that the T18N point mutation is more soluble than the wild type, since according to the hydrophobic character of the residues [40], THR is a more hydrophobic residue than ASN. This is corroborated by a study of Chang et al [41] on solvation free energies of amino-acids in water, in which the difference in solvation free energies was found to be 5 kcal/mol or, equivalently around 10 k_BT. This led us to hypothesize that the IBS surface of the WT, which is (part of) the more hydrophobic side of the protein, is therefore more likely to be adsorbed at the air-water interface, compared to the mutant. Hence, it is conceivable that the wild type AFP protein has a different preferred orientation at the air water surface than the mutant proteins, resulting in less hydration of the IBS for the wild type compared to the mutant IBS. Before embarking on large scale MD simulations of preferential protein adsorption at an air-water interface, we first investigate the protein-water dynamics for a system with a (much) reduced degree of hydration, mimicking this adsorption. We therefore performed MD simulations with a reduced water content of 10% of the fully hydrated system. The remaining 722 waters initially hydrate the entire protein surface, but quickly reorganize, leading to partial exposure to the gas phase due to the hydrophobicity of these parts. In particular, the hydrophobic patch of the protein surface near the IBS became exposed (see Fig. 9 for snapshot). It is thus likely that this part of the surface becomes exposed at the air-water interface. Nevertheless, the IBS is not completely water free, and we can analyze our system in the same way as for the fully hydrated system. Therefore, we measure again the structural parameter S, the reorientation time τ and the hydrogen bond life time τ_{HB}, and compare them in Fig. 10). Clearly, the dehydrated WT shows a strong increase both in water structure and reorientation time at the THR-18, although not so much in τ_{HB}.

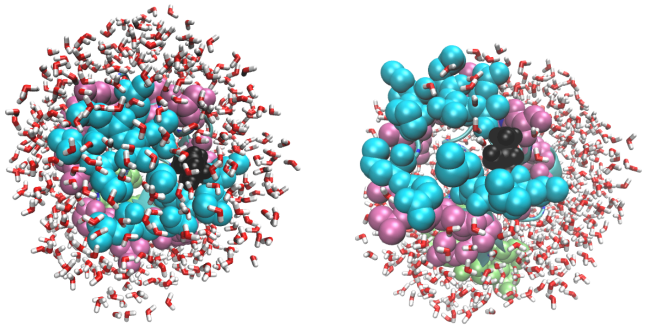

Fig. 9 Starting frame of dehydrated NVT system (left) and a dehydrated protein at a frame after 100 ns (right). Protein color coding as in Fig. 1.

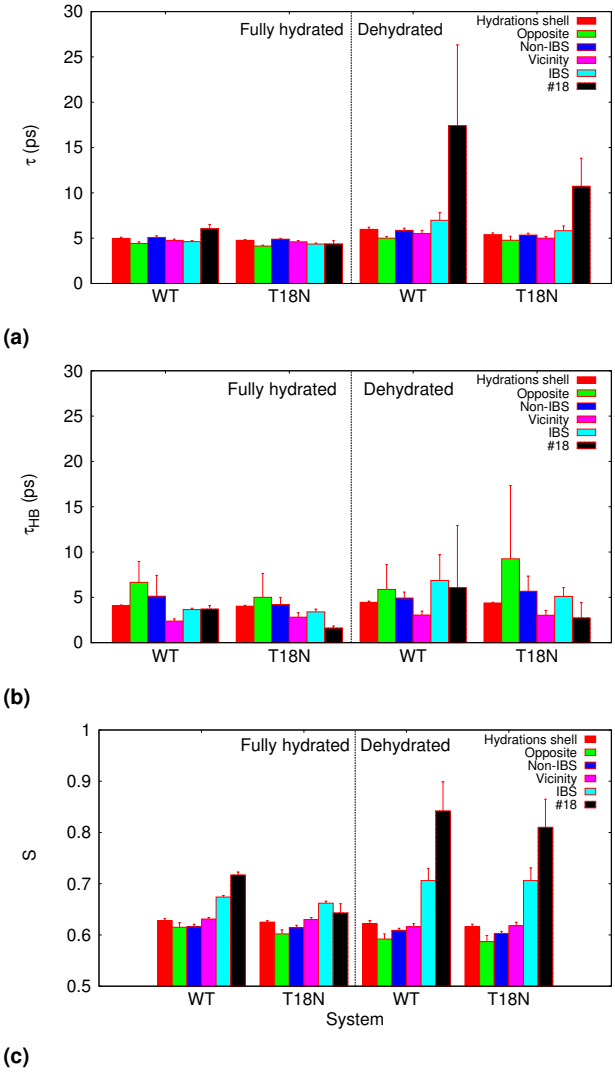

Fig. 10 a) Water reorientation time, b) protein water H-bond lifetimes, and c) structural parameter S of hydration water for SPC/E systems of a fully hydrated wild type and mutant, and for dehydrated wild type and mutant at room temperature.

Comparing the 100 ns NVT simulations of the SPC/E dehydrated wild type and mutant systems at room temperature, on average there are 44 water molecules within 4.4 Å of the wild type IBS, compared to 50.41 for the mutant IBS. There are on average 4.6 water molecules present around THR 18 and on average 5.3 water molecules around ASN-18 of the mutant, indeed suggesting an increase of solvation upon mutation. Therefore, to assess whether differences in hydration contribute to the strong ice-like signal in VSFG experiments, one should compare the dehydrated wild type IBS, THR-18 water structure to the fully hydrated mutant IBS, ASN-18 water structure. Indeed, the dehydrated wild type S_{IBS},S_{18} is significantly higher than the relevant structural parameter S of the fully hydrated mutant (see Fig. 10c).

One could argue that the dehydrated simulations are not representative of a flat air-water interface as present in the experiments, and that the difference in hydration might be insufficient to explain the difference in adsorption at the air water interface.

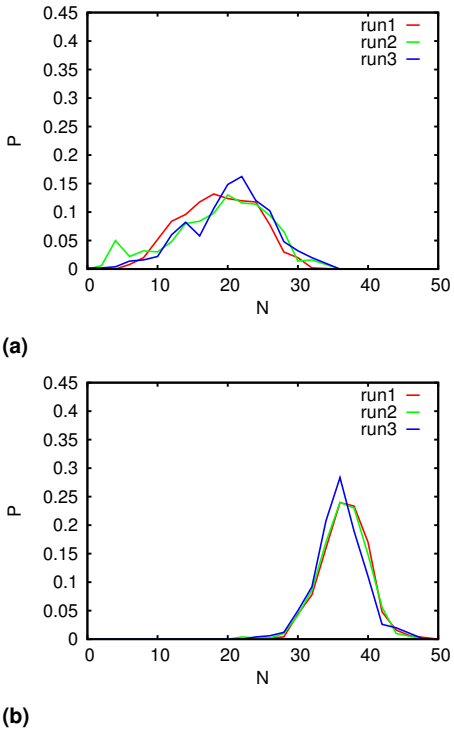

Fig. 11 Distribution of number of water molecules within 0.65 nm of THR-18 and ASN-18 for a) WT slab geometry and b) T18N slab geometry respectively. Hydration for different radii of 0.45 nm and 0.55 nm are reported in Figure S54. Note that the THR-18 is less hydrated than ASN-18 for all different radii used.

Therefore we further tested our hypothesis by simulating the WT and T18N systems explicitly at the water-air interface by setting up a slab geometry in a rectangular box at room temperature, creating a coexistence between water and vapor (see Methodology). Initially located at the center of the ~ 5.8 nm wide water slab the protein relocates and effectively adsorbs at the water-air interface during a 100 ns NVT run, either at the top interface, or the bottom interface (see Figure S24). In Fig. 11 we report the level of hydration of THR-18 and ASN-18 by identifying the number of waters within 0.65 nm of THR-18 and ASN-18 respectively. Both Fig. 11 and Figure S25 indicate that the WT protein adsorbs at the air water interface with THR-18 being most likely exposed towards the air (with a corresponding smaller hydration), whereas the T18N protein adsorbs to the surface with the ASN-18 most likely pointing away from the air-water, and is thus fully hydrated.

The different adsorption properties of the two proteins, in combination with their hydration layer properties provide a plausible explanation for the strong observed difference in the experimental VSFG signal[17]. The wild type has its IBS surface with its structured water exposed to the air water interface, thus leading to a strong signal. The mutant's IBS surface is turned away from the air-water surface, therefore its structured water will contribute much less to the VSFG signal. Instead, other parts of the protein that have less ordered water are now exposed to air, giving rise to a weaker signal.

4 Conclusions

Antifreeze proteins (AFPs) are believed to prevent ice formation by binding to specific ice crystal planes and blocking their growth. Their ice-binding recognition sites have remarkable solvation properties. Spectroscopic experiments[17] and analysis of crystal structures[20] of the ocean pout AFP III anti-freeze protein indicated that upon mutating THR 18 to ASN-18 water locally to the mutation reduces its tetrahedral structure dramatics, suggesting that THR18 plays a crucial role in the ice binding site, and is able to structure water, leading to an increased AFP III affinity to ice. The structure of a protein's hydration layer is tightly related to its dynamics, but this relation has not been elucidated for AFPs. To investigate this relation we performed molecular dynamics simulations of AFP III. We investigate both dynamics and structure of the ice-binding surface and compared these to the non-ice-binding surfaces. We find that while the hydrogen bond dynamics is not remarkably altered, the reorientation of water molecules hydrating the THR18 residue is slower than that of water molecules hydrating the non ice-binding surface. However, this local slow reorientation relaxation is correlated with longer lived H-bonds between THR-18 and its hydrating water compared to ASN-18 in the mutant. Moreover, by comparing structural signatures we found, in agreement with experiments[17] and predictions[20], that upon replacing THR18 with ASN-18, water around the point mutation reduces its tetrahedral structure. Indeed, the THR18 water tetrahedral structure exhibits a positive correlation with reorientation relaxation time, whereas this positive correlation is significantly reduced for the mutant as well as for the entire IBS of the mutant system. This reduction of the $S-\tau$ (and $q-\tau$) correlation at the IBS of the mutant, enhanced at lower temperatures, could explain the smaller affinity of the mutant IBS to ice. In contrast, we find that positively charged amino acids, such as ARG-39, a positively charged H-bond donating residue in the vicinity of the IBS, shows a negative correlation of water tetrahedral structure and reorientation while some others, can show both a positive and negative correlation (ALA-48). Overall, the water tetrahedral structure increases towards the IBS.

In the VSFG experiments the proteins adsorbed at the surface contribute most to the signal[17]. As these proteins experience a lower degree of hydration we also investigate the effect of hydration. We find that dehydration leads to a strong increase in the tetrahedral nature of water, as well as to a strong increase in the time constant of reorientation dynamics. Indeed the THR-18 of the WT compared to ASN-18 of the T18N, has a higher affinity towards air at a slab, thus leading to a more dehydrated solvation, which we find has a much higher tetrahedral structure water surrounding it.

Our findings show that amino acids can act as water tetrahedral structure makers and breakers. This may explain the mechanism of ocean pout AFP to prevent engulfment within an growing ice crystal, since the charged residues such as ARG break the ice structure and induce more glass-like behavior around the IBS, thereby preventing ice from covering the whole protein and inactivating the AFP.

5 Acknowledgement

The research leading to these conclusions was funded the NanoNextNL Programme, a micro and nanotechnology consortium of the Government of the Netherlands and 130 partners. We acknowledge support from the Nederlandse Organisatie voor Wetenschappelijk Onderzoek (NWO) for the use of supercomputer facilities. IKV is grateful for the financial support by the European Union (ERC-2014-StG Contract No. 635928) and the Dutch Science Foundation (NWO ECHO Grant No. 712.016.002).

References

1 S. Bandyopadhyay, S. Chakraborty and B. Bagchi, *J. Am. Chem. Soc.*, 2005, **127**, 16660–7.

2 R. K. Eppler, R. S. Komor, J. Huynh, J. S. Dordick, J. A. Reimer and D. S. Clark, *Proc. Natl. Acad. Sci. U.S.A.*, 2006, **103**, 5706–5710.

3 M. Grossman, B. Born, M. Heyden, D. Tworowski, G. B. Fields, I. Sagi and M. Havenith, *Nat. Struct. Mol. Biol.*, 2011, **18**, 1102–8.

4 J. A. Raymond and A. L. Devries, *Proc. Natl. Acad. Sci. U.S.A.*, 1977, **74**, 2589–2593.

5 A. S. Oude Vrielink, A. Aloi, L. L. C. Olijve and I. K. Voets, *Biointerphases*, 2016, **11**, 018906–018916.

6 A. L. Rubinsky, B. and Arav, A. and De vries, *Cryobiology*, 1992, **29**, 69–79.

7 L. C. Dai H, Guo S, *Shipin Yu Fajiao Gongye*, 2001, **27**, 44–49.

8 C. Yang and K. a. Sharp, *Biophys. Chem.*, 2004, **109**, 137–148.

9 K. R. Gallagher and K. A. Sharp, *Biophys. Chem.*, 2002, **105**, 195–209.

10 N. Smolin and V. Daggett, *J. Phys. Chem. B*, 2008, **112**, 6193–6202.

11 J. Baardsnes and P. L. Davies, *Biochim Biophys Acta*, 2002, **1601**, 49–54.

12 A. B. Siemer, K.-Y. Huang and A. E. McDermott, *Proc. Natl. Acad. Sci. U.S.A.*, 2010, **107**, 17580–17585.

13 E. I. Howard, M. P. Blakeley, M. Haertlein, I. Petit-Haertlein, A. Mitschler, S. J. Fisher, A. Cousido-Siah, A. G. Salvay, A. Popov, C. Muller-Dieckmann, T. Petrova and A. Podjarny, *J. Mol. Recognit.*, 2011, **24**, 724–32.

14 J. Baardsnes, L. H. Kondejewski, R. S. Hodges, H. Chao, C. Kay and P. L. D. Y, *FEBS Lett.*, 1999, **463**, 87–91.

15 A. Cheng and K. M. Merz, *Biophys. J.*, 1997, **73**, 2851–73.

16 D. R. Nutt and J. C. Smith, *J. Am. Chem. Soc.*, 2008, **130**, 13066–13073.

17 K. Meister, S. Strazdaite, A. L. DeVries, S. Lotze, L. L. C. Olijve, I. K. Voets and H. J. Bakker, *Proc. Natl. Acad. Sci. U.S.A.*, 2014, **111**, 17732–17736.

18 S. Pronk, S. Páll, R. Schulz, P. Larsson, P. Bjelkmar, R. Apostolov, M. R. Shirts, J. C. Smith, P. M. Kasson, D. van der Spoel, B. Hess and E. Lindahl, *Bioinformatics (Oxford, England)*, 2013, **29**, 845–54.

19 A. A. Antson, D. J. Smith, D. I. Roper, S. Lewis, L. S. Caves, C. S. Verma, S. L. Buckley, P. J. Lillford and R. E. Hubbard, *J. Mol. Biol.*, 2001, **305**, 875–89.

20 S. Graether, C. DeLuca and J. Baardsnes, *J. Biol. Chem.*, 1999, **274**, 11842–11847.

21 C. Vega and J. L. F. Abascal, *Phys. Chem. Chem. Phys.*, 2011, **13**, 19663–88.

22 Z. F. Brotzakis, C. C. M. Groot, W. H. Brandeburgo, H. J. Bakker and P. G. Bolhuis, *J. Phys. Chem. B*, 2016, **120**, 4756–4766.

23 K. Lindorff-Larsen, S. Piana, K. Palmo, P. Maragakis, J. L. Klepeis, R. O. Dror and D. E. Shaw, *Proteins*, 2010, **78**, 1950–8.

24 G. Bussi, D. Donadio and M. Parrinello, *J. Chem. Phys.*, 2007, **126**, 014101–7.

25 M. Parrinello, *J. Appl. Phys.*, 1981, **52**, 7182–7190.

26 A. Luzar and D. Chandler, *Phys. Rev. Lett.*, 1996, **76**, 928–931.

27 R. Kumar, J. R. Schmidt and J. L. Skinner, *J. Chem. Phys.*, 2007, **126**, 204107–1–204107–12.

28 E. Duboué-Dijon and D. Laage, *The Journal of chemical physics*, 2014, **141**, 22D529.

29 W. H. Brandeburgo, T. V. D. Post and J. Meijer, *Phys. Chem. Chem. Phys.*, 2015, **17**, 24968–24977.

30 G. Lipari and A. Szabo, *Biophys J*, 1980, **30**, 489–506.

31 H. J. Bakker and J. L. Skinner, *Chem. Rev.*, 2010, **110**, 1498–517.

32 B. Madan and K. Sharp, *J. Phys. Chem.*, 1996, **100**, 7713–7721.

33 K. A. Sharp and J. M. Vanderkooi, *Accounts. Chem. Res.*, 2010, **43**, 231–239.

34 J. Errington and P. Debenedetti, *Nature*, 2001, **409**, 318–321.

35 E. Shiratani and M. Sasai, *J. Chem. Phys.*, 1996, **104**, 7671–7680.

36 G. Stirnemann and D. Laage, *J. Chem. Phys.*, 2012, **137**, 031101–1–031101–4.

37 Y. Xu, A. Bäumer, K. Meister, C. Bischak, A. L. DeVries, D. M. Leitner and M. Havenith, *Chem. Phys. Lett.*, 2015, **647**, 1–6.

38 M. Bar Dolev, I. Braslavsky and P. L. Davies, *Annu. Rev. Biochem.*, 2016, **85**, annurev–biochem–060815–014546.

39 P. Czechura, R. Y. Tam, E. Dimitrijevic, A. V. Murphy and R. N. Ben, *J. Am. Chem. Soc.*, 2008, **130**, 2928–2929.

40 J. Kyte and R. Doolittle, *J. Mol. Biol*, 1982, **157**, 105–132.

41 J. Chang, A. M. Lenhoff and S. I. Sandler, *J. Phys. Chem. B*, 2007, **111**, 2098–2106.

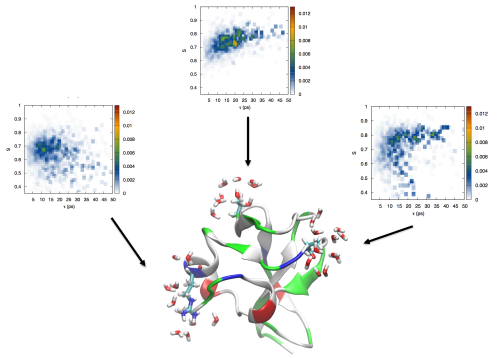

Fig. 12 Signal of anti-correlation of tetrahedral structure of water (S) and its OH reorientation decay time (τ) for selected amino-acids of the Ice Binding Site vicinity (left and right) and positive correlation between the tetrahedral structure of water (S) and its OH reorientation decay time (τ) of the Ice Binding Site central amino-acid (middle).